ADVANCED ENERGY MATERIALS
www.advenergymat.de

A Solution-Mediated Pathway for the Growth of the Solid Electrolyte Interphase in Lithium-Ion Batteries

*Meysam Esmaeilpour, Saibal Jana, Hongjiao Li, Mohammad Soleymanibrojeni, and Wolfgang Wenzel**

Lithium-ion batteries (LIBs) are a widely used battery technology. During the initial LIB cycle, a passivation layer, called the solid electrolyte interphase (SEI), forms on the anode surface, which plays a crucial role in the performance and long-term cyclability of LIBs. The overall mesoscale mechanisms of SEI formation and its composition remain elusive both in experimental and computational approaches. Here a multiscale approach to comprehensively characterize the growth and composition of the SEI based on a chemistry-specific reaction network is presented. Generating an ensemble of over 50 000 simulations representing different reaction conditions, it is found that the organic SEI forms and grows in a solution-mediated pathway by aggregation of SEI precursors far away from the surface via a nucleation process. The subsequent rapid growth of these nuclei leads to the formation of a porous layer that eventually covers the surface. This finding offers a solution to the paradoxical situation that SEI constituents can form only near the surface, where electrons are available, but does not stop growing when this narrow region is covered. The study is able to identify the key reaction parameters that determine SEI thickness, which pave the way to optimize battery performance and lifetime.

1. Introduction

Lithium-ion batteries (LIBs) have been playing a pivotal role in portable devices and electric vehicles in modern society.[1–3] The solid electrolyte interphase (SEI) between anode and electrolyte forms due to the decomposition of the electrolyte, as the operating potentials of the anode (≈0.2 V vs Li^+/Li) are outside the electrochemical stability window of the electrolyte. Understanding the formation, growth and stability of the SEI is essential for optimizing the operation and degradation of all liquid-electrolyte batteries.[4,5] Even though the fundamental interfacial processes and their governing chemistries are well known, the mechanism of formation and degradation of the SEI on the mesoscale (≈50 nm) remains elusive.[6,7] Overall, the SEI is still considered "the most important but least understood" component of batteries.[4,7,8]

The SEI initially forms on the anode during the first few cycles of battery operation.[9] Many electrolytes for LIBs include a salt of Li (e.g., $LiPF_6$) dissolved in carbonate solvents such as ethylene carbonate (EC) and various additives.[10] During the first charging of the LIBs, EC is reduced and decomposed in presence of Li^+ ($LiPF_6$) on the anode surface in several steps. The reaction products form an SEI layer composed of thin inorganic and organic SEI clusters.[7,11] In principle, this reaction cycle would continue indefinitely, but the reaction products ultimately participate in the growth of the SEI, a heterogenous film with an inorganic-rich inner layer and an organic-rich outer layer,[12] which blocks further reactions. The dynamic evolution of the early-stage inorganic SEI proceeds via autocatalytic hydrolysis of electrolytes triggered by the reduction of trace impurities (such as H_2O, HF, etc.), which may lead to continuous growth in thickness etc. during cycling.[9,12–14] Presently, the precise structure, composition, morphology as well as the mechanisms of SEI remain under debate, in particular regarding the mechanism of its growth. In recent years, with the development of in-situ characterization technologies,[8] including secondary-ion-mass-spectroscopy,[15] atomic force microscopy (AFM),[16] electrochemical quartz microbalance,[7] etc. the SEI composition as well as the early stages of SEI formation could be studied in greater detail. However, these technologies are still limited in the exploration of practical battery interfaces, especially in the long-term cycling due to the extreme chemical sensitivity of SEI toward oxygen and hydrogen, as well as the specific locations of SEI which are difficult to access by present instruments.[17,18]

It is well known that the SEI growth spans multiple time- and length-scales. Many theoretical studies have focused on the electrochemistry at the molecular level, elucidating the thermodynamic and kinetic properties of the solvents at the quantum chemistry level.[2,9] These methods explain a variety of phenomena, such as why adding vinylene carbonate (VC) in EC forms a much better SEI than without VC, and it is due to the preferential reactions of additive VC with the EC anion radical

M. Esmaeilpour, S. Jana, H. Li, M. Soleymanibrojeni, W. Wenzel
Institute of Nanotechnology
Karlsruhe Institute of Technology
Hermann-von Helmholtz-Platz 1, D-76344 Eggenstein-Leopoldshafen, Germany
E-mail: wolfgang.wenzel@kit.edu

The ORCID identification number(s) for the author(s) of this article can be found under https://doi.org/10.1002/aenm.202203966.

© 2023 The Authors. Advanced Energy Materials published by Wiley-VCH GmbH. This is an open access article under the terms of the Creative Commons Attribution-NonCommercial License, which permits use, distribution and reproduction in any medium, provided the original work is properly cited and is not used for commercial purposes.

DOI: 10.1002/aenm.202203966

to suppress the 2e reduction of EC.[19,20] But, at a larger scale, there is little understanding of the consequences of the molecular processes. Molecular dynamics (MD) simulations coupled with reactive force field methods could illustrate the growth of the SEI on the scale of a few nanometers,[21,22] but the simulation is constrained to the very early stage of SEI formation due to the time limitation of MD methods. Beyond the nearly-atomistic scale, many phenomenological models mostly employ the continuum methods that attempt to elucidate the growth of the SEI on a larger scale.[23,24]

However, these methods struggle to resolve the apparent growth-paradox of SEI formation: Decomposition of the electrolyte requires electrons, which are supplied from the anode. There is strong evidence that the tunneling depth of the electrons into the organic solvent is only around 2–3 nm.[25] This means that the products of electrolyte decomposition form near the anode surface, where their aggregation into an SEI layer should eventually block the generation of new SEI. In such a scenario, which is termed the near-shore scenario,[26] the SEI should not grow significantly beyond the scale of a few nanometers. Experimental observations indicate that this is true for the inorganic SEI, but not for the organic SEI, which grows to a thickness of 50–100 nm.[27–29] Because continuum models cannot resolve the local structure of the SEI, various mechanisms have been postulated to overcome this apparent paradox: Some authors assume that the SEI is porous, which would confine the growth of new SEI to the pores of the material that has already been formed.[30–33] However, this idea fails to solve the paradox; it merely transfers it from the total volume near the anode to the volume of the pores: As the pores are clogged, the growth of the SEI ceases, again on a scale of a few nm. Other authors argue that the SEI is electronically conducting, but the microscopic nature of this conduction mechanism remains unclear, because the organic SEI forms from electronically insulating degradation products of the electrolyte.[32,34,35] Therefore, we lack a microscopic understanding of the growth of the SEI on the mesoscale, but it is clear that the growth mechanism has a significant impact on the nature and mechanical stability of the SEI, which limits the lifetime, performance, and safety of LIBs.

In order to address this question, we formulate a bottom-up multiscale approach for the growth of the SEI based on system-specific characterization of the microscopic processes that lead to SEI formation. Based on reaction rates derived from quantum chemical calculations, we systematically explore the growth of the SEI in a mesoscopic model with molecular resolution. We have developed a kinetic Monte Carlo (KMC) protocol that follows the spatiotemporal evolution of organic and inorganic components of the SEI governed by a set of chemical reactions, diffusion, and aggregation with nanometer resolution based on kinetic information computed for specific electrolyte-anode chemistries. Because the transfer of molecular information to the mesoscale introduces a systematic uncertainty in the result of the simulations at the mesoscopic level, we have systematically varied the parameters around the computed values in over 50 000 KMC simulations and classified the growth and composition of the resulting SEI for each set of conditions. We find there are three regions in parameter space which can be classified as resulting in an inorganic-only, "bad" and "good" SEI, the former growing into a very thin, porous, often discontinuous organic layer while the latter constitutes a thick, continuous organic layer. In all scenarios that result in a "good" SEI, we find that the SEI forms via a solution-mediated pathway via the nucleation of SEI precursors far away from the anode surface, followed by rapid subsequent growth of the SEI layer. An analysis of the key reactions along this process enables us to identify the crucial reactions that determine the thickness of the SEI, which forms the basis of a rational design of the SEI for liquid-electrolyte batteries.

2. Computational Methods

2.1. KMC Model

In order to model the growth of the SEI on the scale of tens of nanometers on timescales approaching hundreds of microseconds, we have implemented KMC (**Scheme 1**) with a resolution of an individual molecule (≈1 nm). KMC is a variant of the Monte Carlo method intended to simulate the time evolution of mesoscale processes where the underlying system decomposes into spatially and temporally discrete states, which then evolve according to a set of transformations, or "reactions". Here, we report results for a 2D model on a square lattice, where space is discretized at a scale commensurate with the dimension of the molecular components, such as dilithium ethylene dicarbonate (Li_2EDC), lithium carbonate (Li_2CO_3), and $C_2H_4OCOOLi$ (≈1 nm). We performed simulations on 2D square lattices with dimensions 50×50 or 100×100, where one edge of the system represents the anode and the opposite edge of the system is modeled as an open absorbing boundary condition, that is, all components diffusing through this boundary leave the system irreversibly. Each site can represent either a solvent-Li complex (EC-Li^+ colored white in the plot) or the result of a reaction between adjacent sites, as listed in **Table 1**. In principle, inert sites containing only solvent can be considered, but since these are non-reactive they slow the kinetics of the process but do not affect the overall morphology of the SEI. The simulation proceeds via a rejection-free kinetic Monte Carlo (rfKMC) model known as the BKL algorithm.[36] At each step, the algorithm collects all possible reactions and selects one to transit to the next state. The occurrence rate for the transition reaction from i to j is calculated according to the transition state theory (TST).[37]

$$r_{i \to j} = ke^{(-E_b/k_B T)} \tag{1}$$

where k is the frequency of atomic vibration, which is taken as 6.25×10^{12} s^{-1}, E_b is the energy barrier for the reaction, k_B is the Boltzmann constant, and T is the temperature.

2.2. Reaction Network

There are a number of reactions that are known to contribute to the growth of the SEI (Table S1, Supporting Information): The molecular components of the SEI are formed by two

© 2023 The Authors. Advanced Energy Materials published by Wiley-VCH GmbH

16146840, 2023, 14, Downloaded from https://onlinelibrary.wiley.com/doi/10.1002/aenm.202203966 by Karlsruher Inst F. Technologie, Wiley Online Library on [11/07/2023]. See the Terms and Conditions (https://onlinelibrary.wiley.com/terms-and-conditions) on Wiley Online Library for rules of use; OA articles are governed by the applicable Creative Commons License

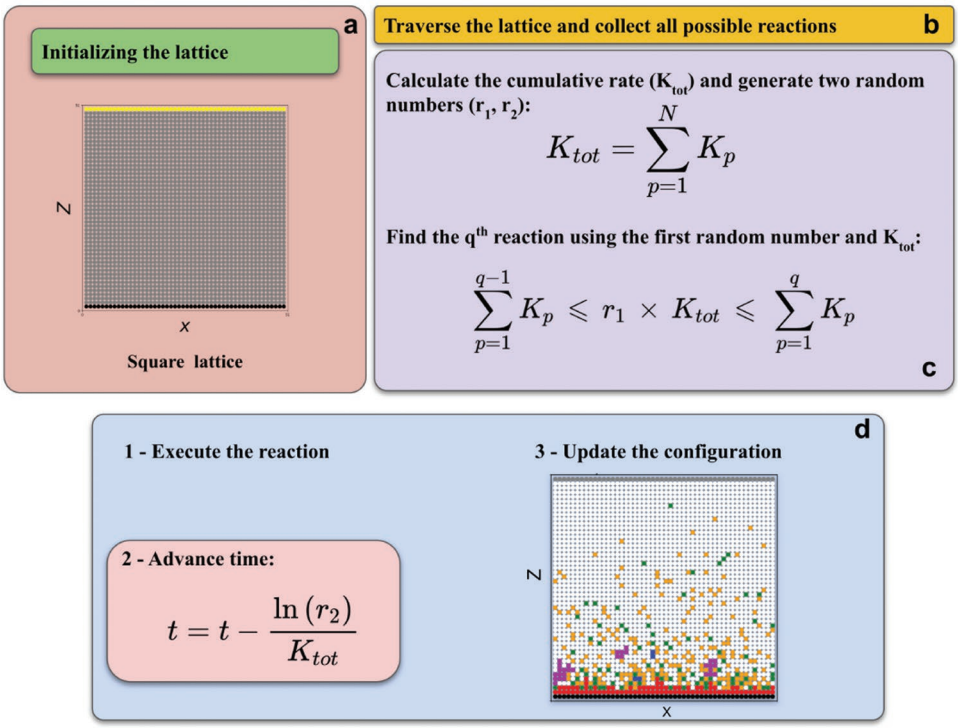

Scheme 1. Schematic depiction of the 2D KMC algorithm for the formation and growth of the SEI on the graphite electrode surface. a) Initializing the lattice, b) collecting all possible reactions, c) selecting a reaction, 4) executing the selected reaction, updating the simulation time, and the lattice configuration. Here, r_1, r_2 are random numbers, K_p is the rate for the pth reaction, and K_{tot} is the cumulative rate over all possible reactions at each step.

consecutive electron reduction reactions of EC molecules that coordinate Li^+ (EC-Li^+).[38,39] Here, we consider only EC-Li^+ as an active medium for the Li diffusion in solvent-mediated pathway. Under the assumption that the SEI is not electronically conducting these reactions can occur only in regions of space where electrons are available, that is, within 4 nm (layers) of the electrode surface

$$\text{Electrode(surf)} + \text{EC} - \text{Li}^+ \rightarrow \text{C}_2\text{H}_4\text{OCOOLi} \quad (2)$$

A second reaction then transforms the product of reaction 1 into inorganic components of the SEI. The generation of Li_2CO_3 can only occur on the anode or on the Li_2CO_3 surface within 4 nm from the anode surface.

$$\text{Electrode(surf)} + \text{C}_2\text{H}_4\text{OCOOLi} + \text{Li}^+ \rightarrow \text{Li}_2\text{CO}_3 + \text{C}_2\text{H}_4 \uparrow \quad (3)$$

$$\text{Li}_2\text{CO}_3\text{(surf)} + \text{EC} - \text{Li}^+ \rightarrow \text{C}_2\text{H}_4\text{OCOOLi} \quad (4)$$

At present, we ignore the gas as it diffuses very fast and leaves the simulation box. Reaction 4 generates the molecular constituents of the organic part of the SEI.

$$\text{C}_2\text{H}_4\text{OCOOLi} + \text{C}_2\text{H}_4\text{OCOOLi} \rightarrow \text{Li}_2\text{EDC} + \text{C}_2\text{H}_4 \uparrow \quad (5)$$

With the exception of Li_2CO_3, which we model to spontaneously aggregate at the anode to form the inorganic part of the SEI, these products of these reactions diffuse in solution.

$$\text{Li}_2\text{EDC} + \text{Li}_2\text{EDC} \rightarrow (\text{Li}_2\text{EDC})_2 \quad (6)$$

In order to model the formation of the SEI, its molecular precursors can aggregate. We model the aggregation in two conceptual steps: Two Li_2EDC can form a dimer (reaction 5). Formation of Li_2EDC dimer as the first SEI agglomeration.

Table 1. List of reactions and their associated rates included in the SEI model.

Entry	Reactants	Products	Initial rate (S^{-1})	Color of product
1	Electrode (surf) + EC-Li^+	$C_2H_4OCOOLi$	1.26×10^9	Green
2	Electrode (surf) + $C_2H_4OCOOLi$ + Li^+	Li_2CO_3 + C_2H_4 ↑	4.43×10^7	Red
3	Li_2CO_3 (surf) + EC-Li^+	$C_2H_4OCOOLi$	2.19×10^8	Green
4	$C_2H_4OCOOLi$ + $C_2H_4OCOOLi$	Li_2EDC + C_2H_4 ↑	6.66×10^7	Orange
5	Li_2EDC + Li_2EDC	$(Li_2EDC)_2$	4.34×10^3	Blue
6	$(Li_2EDC)_2$ + Li_2EDC	SEI cluster	8.60×10^4	Purple
7	Li_2CO_3 (surf) + $C_2H_4OCOOLi$ + Li^+	Li_2CO_3 + C_2H_4 ↑	3.33×10^4	Red
8	Li_2EDC + SEI cluster	SEI cluster	1.32×10^5	Purple
9	$(Li_2EDC)_2$ + SEI cluster	SEI cluster	1.33×10^5	Purple
10	$(Li_2EDC)_2$ + $(Li_2EDC)_2$	SEI cluster	1.29×10^5	Purple
11	SEI cluster + SEI cluster	SEI cluster	1.52×10^5	Purple

The source of the rates is documented in the Supporting Information.[40–42] To illustrate the state of the system lattice points in the figures are depicted with different color codes for the reaction products as indicated.

© 2023 The Authors. Advanced Energy Materials published by Wiley-VCH GmbH

16146840, 2023, 14, Downloaded from https://onlinelibrary.wiley.com/doi/10.1002/aenm.202203966 by Karlsruher Inst F. Technologie, Wiley Online Library on [11/07/2023]. See the Terms and Conditions (https://onlinelibrary.wiley.com/terms-and-conditions) on Wiley Online Library for rules of use; OA articles are governed by the applicable Creative Commons License

$$(Li_2EDC)_2 + Li_2EDC \rightarrow \text{SEI cluster} \quad (7)$$

$$Li_2CO_3(surf) + C_2H_4OCOOLi + Li^+ \rightarrow Li_2CO_3 + C_2H_4 \uparrow \quad (8)$$

$$Li_2EDC + \text{SEI cluster} \rightarrow \text{SEI cluster} \quad (9)$$

$$(Li_2EDC)_2 + \text{SEI cluster} \rightarrow \text{SEI cluster} \quad (10)$$

$$(Li_2EDC)_2 + (Li_2EDC)_2 \rightarrow \text{SEI cluster} \quad (11)$$

$$\text{SEI cluster} + \text{SEI cluster} \rightarrow \text{SEI cluster} \quad (12)$$

When three or more Li_2EDC are attached to each other we label the involved sites as a "SEI cluster", which is a constituent of the organic SEI. There are several molecular attachment reactions that lead to the growth of such a SEI cluster (reaction 6, 8–10) and SEI clusters can merge (reaction 11). In the present model, formation of these SEI clusters is irreversible. In addition to the reactions leading to a transformation of the state of adjacent sites into different states, we define "reactions" that merely exchange the states of two sites (diffusion) (see Supporting Information).[40–42] When particles diffuse across the absorbing boundary opposite to the electrode, products irreversibly leave the system. This loss of material approximates the products of electrolyte decomposition that do not form either the organic or inorganic SEI and affects the overall mass-balance of the battery (see Supporting Information). Table 1 shows the most important reactions in our KMC model (Table S1, Supporting Information contains all reactions).

3. Results and Discussion

The process space of SEI formation in the model is defined by the set of reaction rates which we define as the fifteen-dimensional process space vector (PSV). An initial PSV was generated based on rates which were gathered from the literature (see Supporting Information for sources).[40–42] Given the approximations inherent in the model, there is an uncertainty in the value of these parameters when used in the mesoscopic model. Therefore, the initial values in Table 1 can be considered only an approximation of the PSV that corresponds to the growth of the SEI for any real system. Since the realistic PSV is unknown, we employed a statistical method to explore the PSV space of the model in the vicinity of the approximate PSV in a systematic fashion. We generated a set of 50 000 PSV based on a random variation of the initial PSV using Latin Hypercube sampling,[43–45] a design of experiment (DOE) technique, which allows us to explore the parameter space with respect to the properties of the resulting SEI. Each PSV generates a spatio-temporal model that can be analyzed with respect to the properties and kinetics of the growth of the resulting SEI.

3.1. SEI Growth in a Model System

Before we discuss the characteristics of the resulting growth regimes of the SEI, it is instructive to analyze the spatio-temporal evolution of a single PSV to illustrate the formation and growth of the SEI. **Figure 1** illustrates six different snapshots of simulations for a representative PSV at different simulation times (rates are given in the Supporting Information).[40–42] Note that these times should be interpreted as relative, not absolute values. At the beginning of the simulation (Figure 1a), the first electron reduction reaction of EC-Li^+ starts on the electrode surface and generates $C_2H_4OCOOLi$ (green). These intermediate components diffuse and participate in reactions among themselves or in a second one-electron reduction reaction at the surface of the electrode. As a result of the second one-electron reduction at the electrode surface, $C_2H_4OCOOLi$ (green) transforms to Li_2CO_3 (red), an inorganic SEI component which is observed first around 2 µs of simulation time in the presence of excess Li^+. This inorganic SEI forms an immobile layer on the electrode surface within a very few µs of simulation time and reduces further reduction reactions for the decomposition of the solvents, because it reduces the availability of electrons in the solution. Also, $C_2H_4OCOOLi$ (green) reacts to form Li_2EDC (orange), an intermediate precursor for SEI growth. Li_2EDC (orange) starts to dimerize at around 20 µs of simulation time to form $(Li_2EDC)_2$ (blue), the most essential intermediate for the organic SEI. But, due to the low dimerization rate, the formation of the $(Li_2EDC)_2$ is slow.

At around 94 µs (Figure 1b), a large number of intermediate components, $C_2H_4OCOOLi$ (green), react to form Li_2EDC (orange), and a few dimers $(Li_2EDC)_2$ (blue). All three intermediate components originate near the electrode surface. Due to the high diffusion rate, these SEI precursors diffuse far away from the electrode and distribute almost evenly in the simulation box; some diffuse out of the diffusion box. In this simulation only 63% of the precursors remain inside the simulation box and participate in nucleation, aggregation and deposition. In the representative PSV, the first SEI cluster starts to build via nucleation of two dimers ($(Li_2EDC)_2$, blue) at 160 µs. We find that the nucleation starts not directly at the anode, but at a distance ≈20 nm away from the electrode surface. This is the first evidence of the solution mediated SEI growth mechanism. There are only two possible nucleation mechanisms for the initial SEI clusters (purple); interaction between $(Li_2EDC)_2$ (blue) with either $(Li_2EDC)_2$ (blue) or Li_2EDC (orange) which diffuse through the entire system. Due to the significant reaction rate difference, the first pathway dominates the second. As a result, low concentration $(Li_2EDC)_2$ (blue) eventually nucleates a SEI cluster (purple). Once the SEI clusters (purple) is nucleated, it diffuses slowly, but grows rapidly (within 50 µs simulation time) inwards from these nuclei (see Figure 1c–e). Finally, it touches the surface of inorganic SEI and becomes part of a porous immobile layer of SEI. In the final snapshot (see Figure 1f) at 2.6 ms, the SEI blocks access to the electrode and almost all intermediate components have deposited on either the electrode surface or on the thick SEI layer. Because educts can no longer reach the electrode, the growth of the SEI stops. For this specific choice of PSV, the organic SEI layer dominates the inorganic SEI in volume. The formation of the thin layer of the inorganic SEI results from the slow rates of the second one-electron reduction reactions and the lack of electrons on the surface of the inorganic SEI. The results of the simulations (Figure 1f) agree qualitatively with

© 2023 The Authors. Advanced Energy Materials published by Wiley-VCH GmbH

16146840, 2023, 14, Downloaded from https://onlinelibrary.wiley.com/doi/10.1002/aenm.202203966 by Karlsruher Inst F. Technologie, Wiley Online Library on [11/07/2023]. See the Terms and Conditions (https://onlinelibrary.wiley.com/terms-and-conditions) on Wiley Online Library for rules of use; OA articles are governed by the applicable Creative Commons License

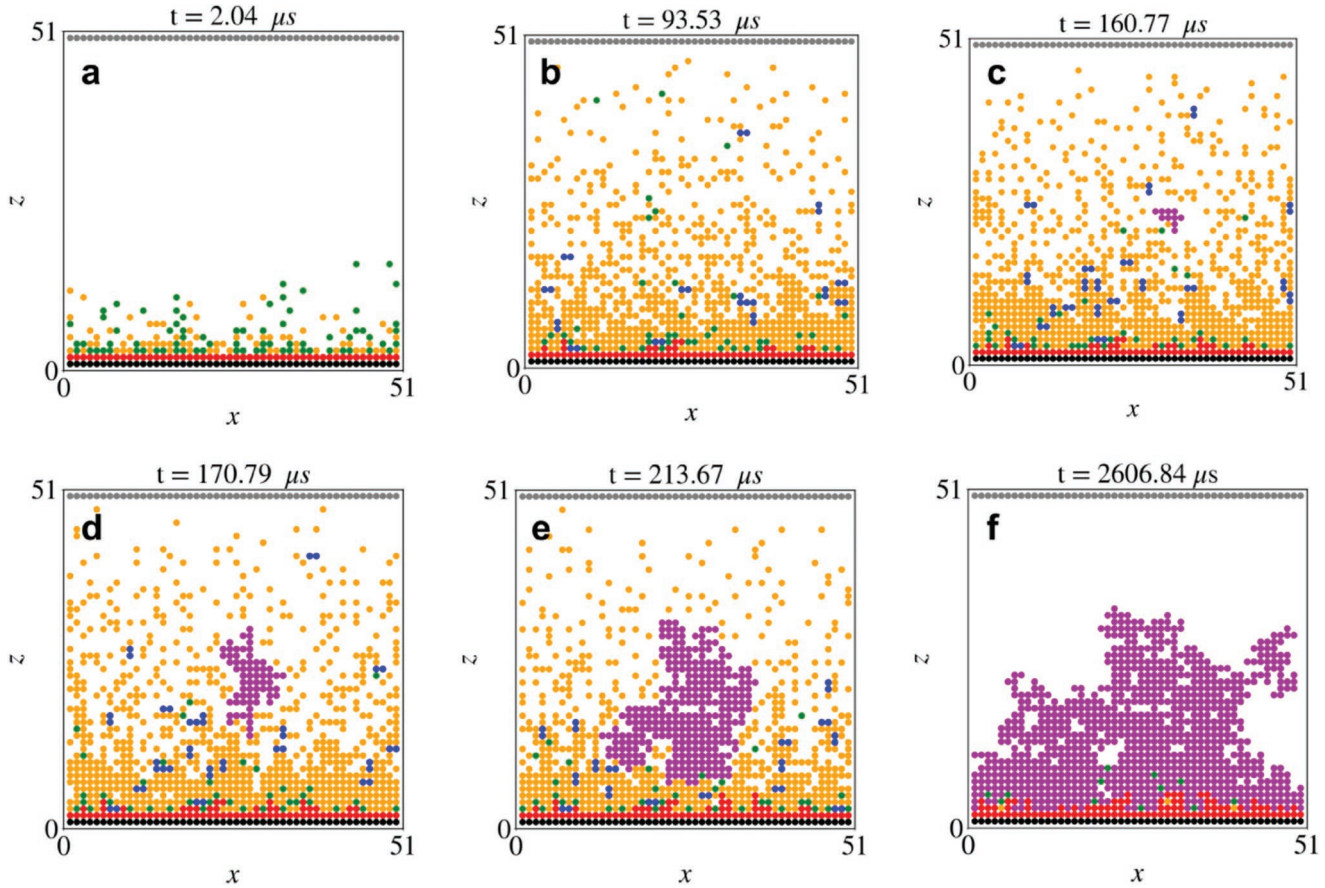

Figure 1. Different snapshots of the KMC simulation (50×50 nm^2) for the representative PSV at the indicated time (see the Supporting Information). In the simulation box, the graphite electrode layer is implemented at the bottom (black), the absorbing open interface at the top. Initially, all other sites are occupied by EC-Li^+ (white), the precursor for the SEI formation at the start of the simulation. The reaction intermediates and products, namely Li_2CO_3, $C_2H_4OCOOLi$, Li_2EDC, $(Li_2EDC)_2$, and organic SEI clusters are represented by red, green, orange, blue, and purple sites, respectively (see Table 1). During the simulation, a) $C_2H_4OCOOLi$ (green) and Li_2EDC (orange) form rapidly a stable inorganic SEI layer (red), and b) Li_2EDC (orange) dimerized to form $(Li_2EDC)_2$ (blue). SEI clusters (purple) start to grow c–e) away from the electrode presence of $(Li_2EDC)_2$ and Li_2EDC, and the organic SEI deposited f) on the inorganic SEI to form porous immovable SEI.

experimental observations, where a thin inorganic SEI forms on the top of the anode surface, which is covered by a thick organic SEI.[46]

To understand the variation of the evolution of the concentration of intermediate components during the growth of the SEI, we plot a time series of their concentrations (**Figure 2**). For the representative PSV, we find that the system reaches a steady state after about 200 µs and that the growth of the SEI proceeds in phases on well-separated time scales. At the start of the simulation, one and two-electron reduction products form within a few microseconds (represented by green and red lines). Immediately, Li_2EDC (orange) starts to grow and reaches a maximum concentration at about 100 µs. Due to the similar rate of formation of $C_2H_4OCOOLi$ (green) and conversion from $C_2H_4OCOOLi$ to Li_2EDC (orange), the concentration of the former stays almost constant throughout the simulation. The combination of the concentration and the low dimerization results in the formation dimers of Li_2EDC, that is, $(Li_2EDC)_2$ after a few tens of microseconds. The dimers diffuse in the simulation box and ultimately nucleate into the first SEI cluster (purple line). Once the nucleation has occurred, the SEI cluster grows fast and reaches a steady state after a few microseconds, consuming Li_2EDC (orange). After 200 µs, the simulation has reached a steady state, and intermediate components are either consumed or trapped inside the final products. At this point, all reactions cease, and a stable porous organic SEI has formed on the anode surface.

Before we discuss the various growth regimes in a systematic fashion, we can already draw one conclusion from this analysis: despite the complexity of the reaction network, growth of an appreciable layer of organic SEI appears to require a large concentration of mobile SEI precursors and a nucleation reaction, which needs not be directly at the electrode. When these conditions are fulfilled, the SEI will grow rapidly into a porous layer that covers the electrode.

To understand the importance of the individual reactions for the SEI formation in more detail, we have computed the occurrence of each reaction in the KMC simulation for the representative PSV (**Figure 3**a). Figure 3b shows the average time needed to complete each step - called the residence time of each

© 2023 The Authors. Advanced Energy Materials published by Wiley-VCH GmbH

16146840, 2023, 14, Downloaded from https://onlinelibrary.wiley.com/doi/10.1002/aenm.202203966 by Karlsruher Inst F. Technologie, Wiley Online Library on [11/07/2023]. See the Terms and Conditions (https://onlinelibrary.wiley.com/terms-and-conditions) on Wiley Online Library for rules of use; OA articles are governed by the applicable Creative Commons License

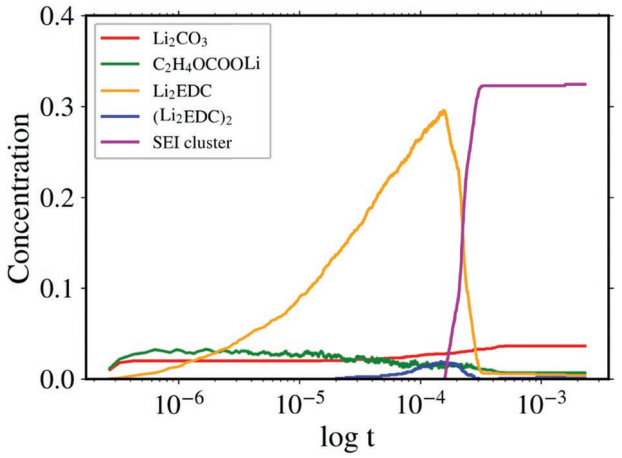

Figure 2. Average concentration of intermediate components and SEI products as a function of time (in seconds) during the spatio-temporal evolution of the reference sample for a given set of reaction rates in the simulation. At the beginning of the simulation, due to electron reductions near the electrode, $C_2H_4OCOOLi$ and Li_2CO_3 components were produced (green and red lines). Both lines rapidly equilibrate (the red line is for the stable inorganic SEI, and the green is for reaching a steady state) with time and the concentration of Li_2EDC rises rapidly. After 20 µs of time, $(Li_2EDC)_2$ (blue line) starts to form as an essential precursor of the SEI cluster (purple line). Once the SEI cluster (purple) has been nucleated, it grows rapidly by consuming Li_2EDC (orange) components. As a result, the Li_2EDC concentration falls rapidly, and all concentrations reach a steady state indicating completion of the SEI formation.

reaction. The product of average residence time and occurrence of each reaction is the total time spent by each particular state (Figure 3c). First of all, we note that the occurrence ratio varies over several orders of magnitude, which is a result of both the reaction rate and the concentration of educts. We concentrate on the occurrence of the reactions that have a critical role during the SEI formation. In order of importance, the most frequent reactions are the first electron reduction, the formation of Li_2EDC from two $C_2H_4OCOOLi$ and all the diffusion processes.

Figure 3a shows that the diffusion of the SEI precursors is critical for a large part of SEI formation. SEI precursors are generated near the electrode-electrolyte interface and diffuse away from the surface. Then these precursors ($(Li_2EDC)_2$) start to nucleate at a distance of about 20 nm. Here, no bar appears for reaction number 6, which means in this simulation no reaction was recorded where Li_2EDC interacts with $(Li_2EDC)_2$ to form SEI clusters. In this simulation nucleation occurs via an interaction between two $(Li_2EDC)_2$.

At the end of the simulation the SEI is approximately 23 nm thick and very few SEI precursors are trapped within the organic SEI. A significant number of vacant lattice points are present within the organic SEI, reflecting its porous nature. Additionally, due to the stochastic growth of the SEI, the surface of the SEI is rough. These characteristics (thickness, porosity, roughness) have a significant role in the mechanical and electrochemical properties of the SEI during battery operation.

The generated SEI consists of a small inorganic layer at the electrode surface, whereas a largest fraction is the organic part of the SEI. The thin inorganic part has almost no defects, while the organic SEI has a porosity of 29%. Mass transport of the precursors of organic SEI away from the surface is a critical step for the nucleation and growth of SEI. In the simulation, the precursors for the organic SEI form near the electrode surface and diffuse away from the surface. After the nucleation reaction, the organic SEI grows from the precursors. Diffusion leads to a significant loss (37%) of the SEI precursors, which leave the simulation cell.

3.2. Classification of the SEI Regimes Using Machine Learning

We have so far used a single PSV to illustrate the mechanisms involved in SEI growth. However, there are many uncertainties that arise from the transfer of electrochemical reaction rates computed in idealized environments into a mesoscale model, such as the one discussed here. In addition, there are assumptions of the model itself, which limit transfer of the parameters, for example, not all species considered have the exactly the same size. Presently, it is very difficult to predictively generate a model by passing parameters from the lower to the more coarse-grained scale, due to the assumptions made on both scales.

While it may not be possible to determine the parameters for a specific chemistry with certainty, we take an alternative approach here: The rate network of the model describes a broad range of chemistries and conditions, each PSV thus constitutes a datapoint in a fifteen dimensional parameter space, which results in different SEI characteristics. In order to obtain a global view on the possible growth scenarios, we performed simulations for a dataset of 50 000 PSV using a design of experiment approach, which systematically varied the parameters to obtain a coverage of this parameter space. For each simulation we computed SEI fraction, porosity and thickness as observables, the whole dataset is available for analysis in MaterialsCloud.

We clustered the dataset using K-Means clustering[46,47] and reduced the dimension using the Uniform Manifold Approximation and Projection (UMAP) algorithm,[48] which resulted in the best separation score of the clusters (around 0.51). Following the clustering, we determined the optimum number of clusters using the elbow method[49,50] and silhouette score[51] which resulted in just three regions of the 15 dimensional parameter space of the model (see Figure S4, Supporting Information). PSV in each of these clusters feature fundamentally different compositions of the SEI at the end of the simulation (see Supporting Information for more detail). Simulations in region 1 (21 109 clusters) result only in inorganic SEI, simulations in region 2 (13 554 clusters) result in organic SEI of low thickness and high porosity, while simulations in region 3 (15 337 clusters) result in an organic SEI of appreciable thickness and high density (**Figure 4**). For future reference, we label these regions as "inorganic", "bad" and "good" SEI.

To quantitatively describe the SEI formed in the three regions, we show thickness and porosity in **Figure 5**. The first row in the multipanel figure represents SEI thickness which increases from region 1 to region 3. In region 1, mostly thin inorganic SEI formed, (mean 3.09 nm). Such a thin SEI layer results from the

© 2023 The Authors. Advanced Energy Materials published by Wiley-VCH GmbH

16146840, 2023, 14, Downloaded from https://onlinelibrary.wiley.com/doi/10.1002/aenm.202203966 by Karlsruher Inst F. Technologie, Wiley Online Library on [11/07/2023]. See the Terms and Conditions (https://onlinelibrary.wiley.com/terms-and-conditions) on Wiley Online Library for rules of use; OA articles are governed by the applicable Creative Commons License

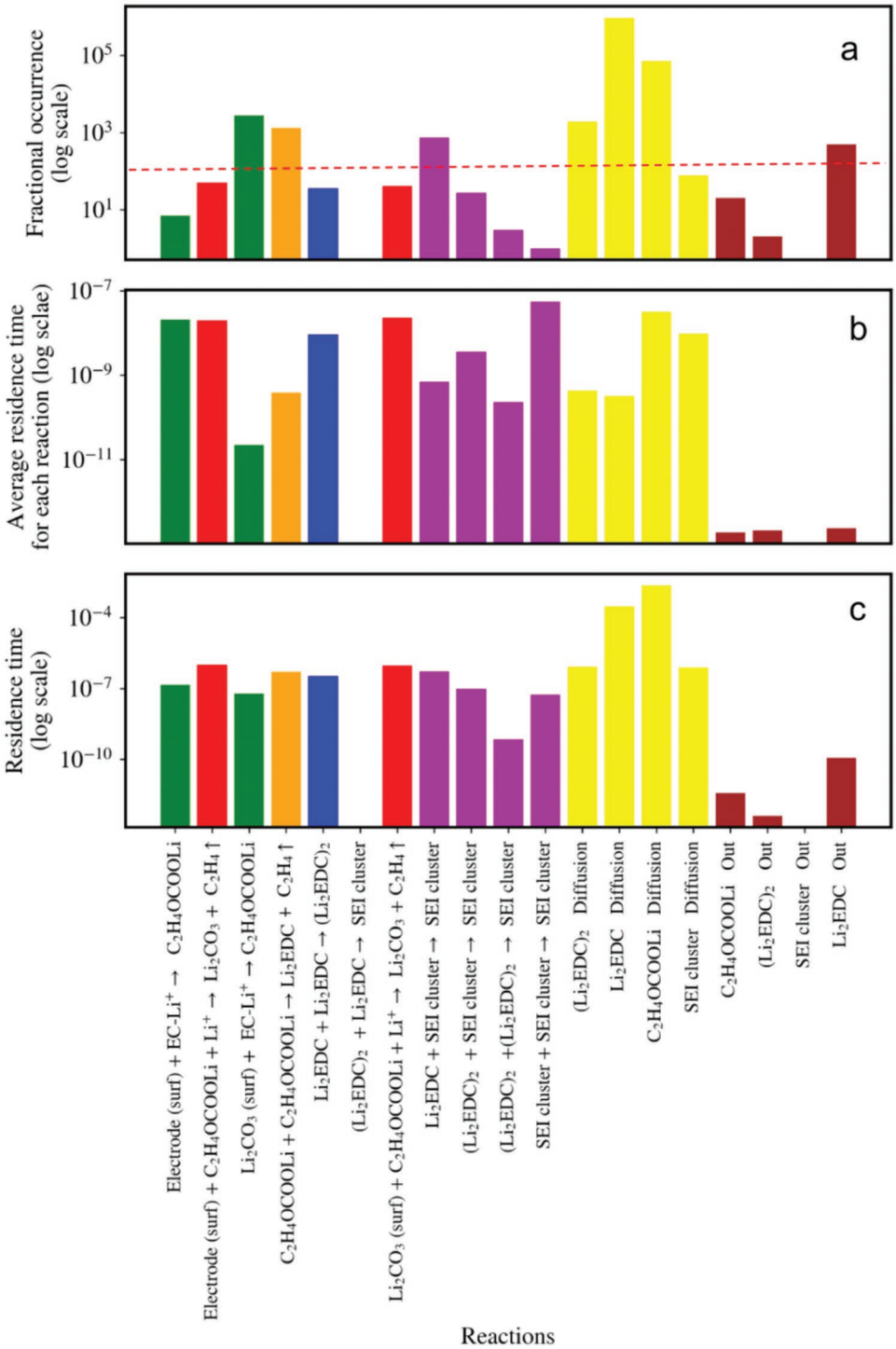

Figure 3. Fractional occurrence and residence time for the reaction in the model for the representative PSV. Here, $C_2H_4OCOOLi$, Li_2CO_3, Li_2EDC, $(Li_2EDC)_2$, and SEI clusters are colored in green, red, orange, blue and purple, respectively. Yellow and brick red bars represent diffusion within and out of the simulation box, respectively. a) Fractional occurrence of each reaction in the simulation. b) Average residence time spent by a particular reaction during the simulation. c) Total residence time spent by each reaction throughout the simulation.

fast inorganic SEI formation and the reduction of available electrons within 4 nm from the anode surface. In region 2, the mean value of SEI thickness slightly increases to around 5.18 nm. In this region we find almost an equal contribution of inorganic and organic parts of the SEI. Notably there is a large portion of the parameter space which results in a thick, albeit porous layer of organic SEI with a mean thickness of 12.14 nm. While this is still less than experimentally observed it is commensurate

© 2023 The Authors. Advanced Energy Materials published by Wiley-VCH GmbH

16146840, 2023, 14, Downloaded from https://onlinelibrary.wiley.com/doi/10.1002/aenm.202203966 by Karlsruher Inst F. Technologie, Wiley Online Library on [11/07/2023]. See the Terms and Conditions (https://onlinelibrary.wiley.com/terms-and-conditions) on Wiley Online Library for rules of use; OA articles are governed by the applicable Creative Commons License

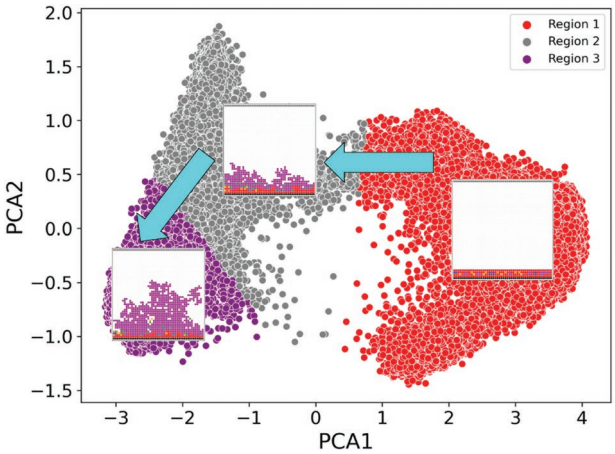

Figure 4. Three different regions of the dataset based on reaction barriers and SEI observables within the parameter space (PSV) along the two most dominant principal components after Principal Component Analysis (PCA) of the clustered dataset comprising (50 000 simulations). The PSV labeled in the region colored in red result in trajectories that have mainly inorganic SEI and no organic SEI, the PSV in the gray region result in thin layers of porous organic and less inorganic SEI. PSV in the purple region result in thick, comparatively dense organic SEI and very thin inorganic SEI.

with the size of the simulation cell (50 nm). The PSV in this region follows a well-defined Gaussian distribution for the SEI thickness.

The clustering of all possible outcomes of the simulations offers us the opportunity to analyze the determinants for the growth of a thick organic SEI. The mean values of the fractional occurrence of the individual reactions for the PSV in region 3 are shown in **Figure 6** (see Figures S5 and S6, Supporting Information for region 1 and region 2, respectively). Note that some reactions occur very infrequently, that is, reaction numbers 5, 6, 7, 9, 10, and 11, which results in large error bars. Here, also we find that diffusion of all precursors for the organic part of the SEI has high occurrences with a large error bar. Though diffusion rates vary significantly from simulation to simulation , diffusion is essential for the formation of "good SEI". This data supports the hypothesis that the mass transport of the reaction products, especially of the organic SEI ingredients (Li_2EDC) drives the formation of a thick and dense SEI. Comparing this figure with Figure 3a, we note striking similarities, which demonstrate that the PSV we selected to illustrate the processes involved in forming the organic SEI is representative for PSV that lead to "good" organic SEI formation. Thus, even though we cannot determine the exact rates for a particular system, we can conclude that "good" organic SEI formation in a model of the general structure discussed here involves a solution mediated, rather than a surface mediated growth mechanism of the organic SEI.

Another consequence of the mass transport pertains to the escape fraction of SEI precursors, defined as the fraction of molecules of a particular species that escape the simulation box versus those that are produced. **Figure 7**a–d shows the escape

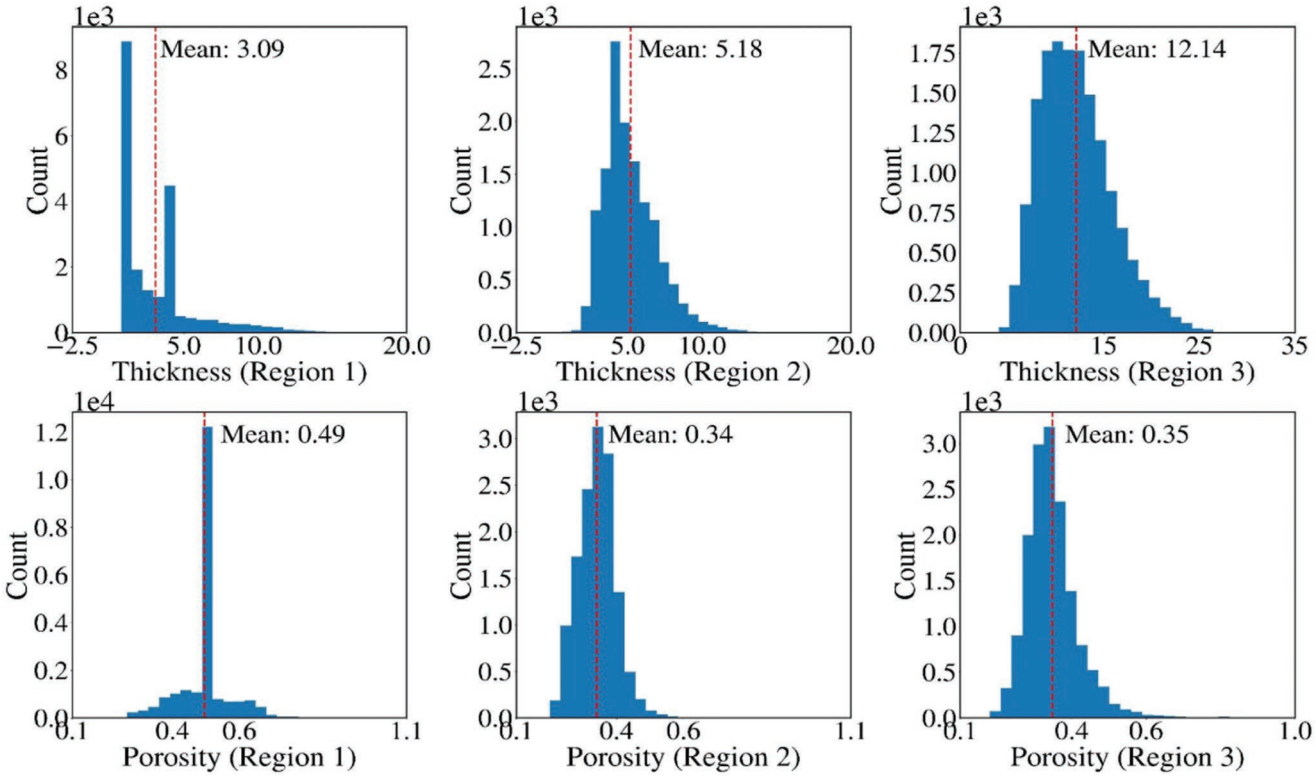

Figure 5. Histograms of a) thickness, b) porosity of the SEI for the three regions of SEI growth (occurence in thousands) (see Figure 4). Here, the red dotted line shows the mean of the observable in each region. The average thickness of the SEI increases from 3.09 nm to 12.14 nm from region 1 to region 3. In contrast, the porosity is similar for all regions.

© 2023 The Authors. Advanced Energy Materials published by Wiley-VCH GmbH

16146840, 2023, 14, Downloaded from https://onlinelibrary.wiley.com/doi/10.1002/aenm.202203966 by Karlsruher Inst F. Technologie, Wiley Online Library on [11/07/2023]. See the Terms and Conditions (https://onlinelibrary.wiley.com/terms-and-conditions) on Wiley Online Library for rules of use; OA articles are governed by the applicable Creative Commons License

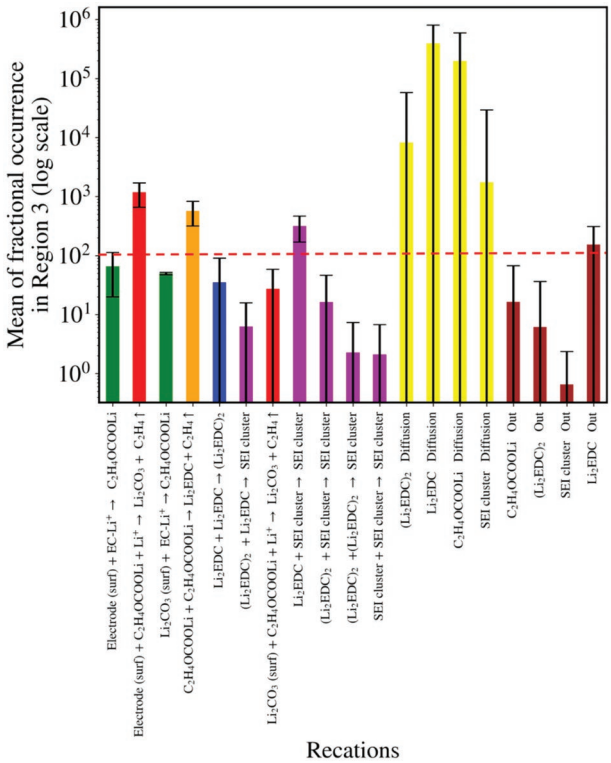

Figure 6. Bar plot for the average fractional occurrence of each reaction in the KMC simulation for region 3 (represents the region for good SEI, see Figure 4). The high mean values for diffusions reflect the necessity to make a good SEI. The error bar represents the standard deviation of the fractional occurrence of the reactions and diffusions. The small error bars are for the frequent fractional occurrence of the reactions, whereas it is the opposite for large error bars.

fraction histogram plot for $C_2H_4OCOOLi$, Li_2EDC, $(Li_2EDC)_2$, and cluster of samples in the region 3 (see Figure S7 and S8, Supporting Information for region 1 and region 2, respectively). Around 1% of $C_2H_4OCOOLi$ escaped out of the system, which means 99% participated in the Li_2EDC production (see Figure 7a). This fraction for Li_2EDC is around 22%, which corresponds to an irreversible loss of SEI precursors before dimerization. For $(Li_2EDC)_2$ and mobile SEI clusters, the escape fraction is around 1% and 0.2%, respectively; which means most of the agglomerated SEI components eventually join the organic SEI cluster to form thick SEI.

To understand the relationship between SEI thickness and the nucleation distance from the electrode surface in more detail, we correlate the distance of the first nucleation event with the thickness of the SEI (**Figure 8**) using the data of region 3 in the dataset. A linear regression fit (Figure 8, blue line) indicates that the thick SEI forms when the nucleation starts far from the surface whenever the thickness of the SEI is large. While the random diffusion of the nucleus has little effect on the final thickness, the agglomeration of material on the nucleus determines the final thickness. The nucleus grows into an SEI particle of ellipsoidal shape according to the distribution of precursors, which diminishes with the distance from the surface. Figure 8 indicates that there is a linear correlation between the distance of this initial nucleation reaction and the thickness of the organic layer of the SEI. This behavior results from the fact that the growth of the SEI approximately stops when the SEI particle touches the electrode, blocking further growth. The slope of this line is less than one, that is, the shape of the growing SEI cluster is elongated in the direction perpendicular to the surface, due to the concentration gradient of the precursors. This data leads us to conclude that the thickness of the SEI is essentially predicted by the distance of the first nucleation reaction. Surprisingly, the SEI is thicker and more robust, the further away the initial SEI cluster is nucleated. In contrast, the porosity of the SEI is similar for all nucleation reactions at different distances from the surface (see Figure S9, Supporting Information). Rapid nucleation near the surface leads to thin layers only (region 2).

This observation offers a simple criterion to control the thickness of the organic SEI, which is the control of the nucleation reactions. Due to computational constraints, we performed all calculations reported here on a 50 nm × 50 nm lattice, which results in SEI of maximally 25 nm thickness.

Another interesting outcome was the correlation between barriers and SEI observables in region 3. **Figure 9** is a visualization of the table of correlation coefficients for some reactions and observables that showed correlations, including the formation of $(Li_2EDC)_2$ and SEI clusters, diffusion of Li_2EDC and SEI clusters, and SEI observables. According to this plot, there is a strong linear relationship between the diffusion of Li_2EDC and the formation of $(Li_2EDC)_2$; and also between the formation of $(Li_2EDC)_2$ and SEI thickness. This emphasizes the importance of dimerization to form the precursor for the nucleation to initiate the first organic ingredients in the solution-mediated SEI growth mechanism.

We finally return to a discussion of the alternative scenarios of SEI growth that were discussed in the introduction. Neither of these mechanisms were observed to promote SEI growth in any of the 50 000 simulations reported here. For the pathway involving electron transport through the organic SEI, our model simply lacks any constituent that can mediate such transport. More importantly, we did not observe any growth of organic SEI through "cracks" or "pores" within the SEI. To quantitatively demonstrate that such a mechanism appears infeasible we performed two additional simulations which would favor such a scenario. We first increased the rate by which lithiated solvent can exchange with organic components. This enables a mechanism where the lithiated solvent can reach the surface of the inorganic SEI or anode for the Li intercalation or solvent reduction reactions. As Figure S10, Supporting Information shows, a thin organic SEI has formed 9 nm away from the anode surface and grows inward very fast and forms a thick organic SEI within 260 µs. Because the lithiated solvent can diffuse through the organic SEI, the latter cracks and separates into small organic clusters and diffuses into the solution. As a result, the organic SEI dissolves, and only the inorganic SEI remains. Since we could not observe SEI growth via this mechanism, we investigated SEI stability: we start with a preformed thick organic SEI and subsequently increase the rate of solvent-SEI exchange. As shown in Figure S11, Supporting Information, we observe a continuous degradation of the organic SEI to a thin layer of less than 3 nm (4 ms). As a result of these simulations we conclude that many diffusive events must take place for a solvent molecule to pass

© 2023 The Authors. Advanced Energy Materials published by Wiley-VCH GmbH

16146840, 2023, 14, Downloaded from https://onlinelibrary.wiley.com/doi/10.1002/aenm.202203966 by Karlsruher Inst F. Technologie, Wiley Online Library on [11/07/2023]. See the Terms and Conditions (https://onlinelibrary.wiley.com/terms-and-conditions) on Wiley Online Library for rules of use; OA articles are governed by the applicable Creative Commons License

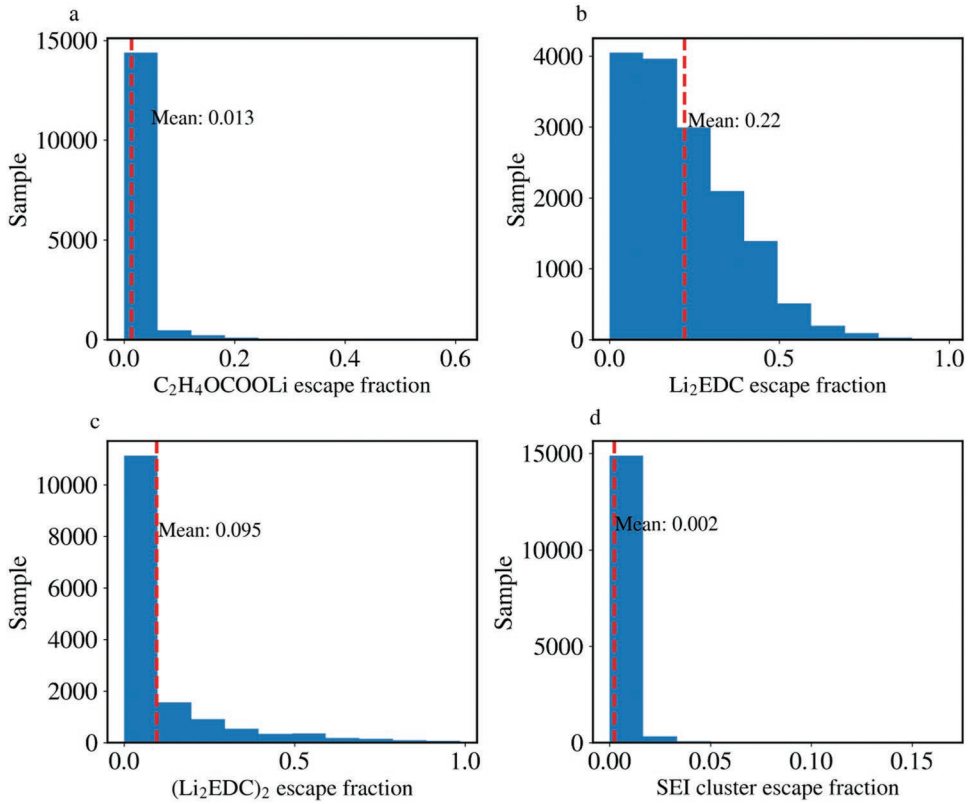

Figure 7. Histograms of escape fraction of organic SEI precursors a) $C_2H_4OCOOLi$, b) Li_2EDC, c) $(Li_2EDC)_2$, and d) SEI clusters, that is, the fraction of precursors that diffuse out of the KMC simulation box for region 3 (see Figure 4). Here, the red dotted line represents the mean escape fraction of the precursors. A low mean value of the escape fraction means that more precursors form the organic SEI. Li_2EDC has the highest escape fraction among these four precursors because competing reactions infrequently occur before nucleation.

through a thick SEI to eventually reach the surface, where it may react and form a single new constituent of the organic SEI. Meanwhile, each of these diffusive events can lead to cracking of the SEI, which in the statistical average leads to much faster degradation than regrowth.

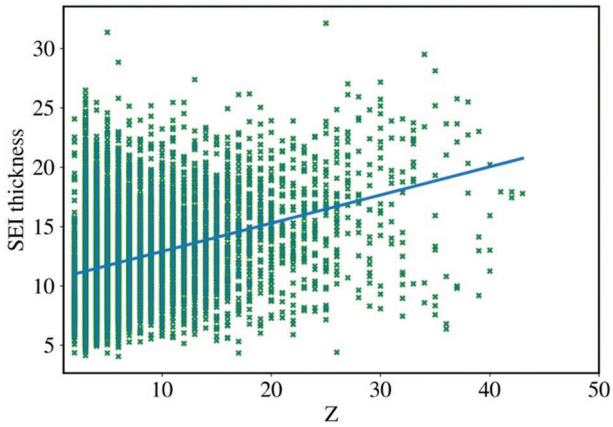

Figure 8. Scatter plot of SEI thickness with respect to the distance (Z) of the first nucleation (formation of a SEI cluster for organic SEI (purple)) from the electrode for the samples in the region 3. The blue solid line is the linear regression fit which indicates that the thickness of the SEI increases with the distance of the first appearance of the SEI clusters. Thicker SEI developed when the nucleation starts far away from the electrode surface, which results from the directional growth through aggregation along a concentration gradient. If the nucleation starts near the electrode then the electrode is rapidly blocked.

4. Conclusions

While it is generally acknowledged that the SEI is one of the most important components of liquid electrolyte batteries, the mechanism of its growth and consequently its structure and function remain enigmatic. Explanations and models for the growth of the SEI must overcome the paradoxical situation that electrons that are required for the electrochemical reactions that degrade the electrolyte into the SEI precursors are available only within a few nanometers of the electrode surface, while the organic SEI in functional batteries is an order of magnitude thicker. In this study, we have presented a multi-scale model that offers a solution to this paradox by postulating a solution-mediated pathway for SEI growth. We constructed a reaction network for the established microscopic reactions that are known to be relevant for the growth of the SEI and obtained an initial set of rates based on literature data. Because the transferability of the microscopic reaction parameters, which are obtained under the idealized assumption to our mesoscopic model, which in turn makes several assumptions, is limited we performed a design-of-experiment study which spanned the relevant parameter space of the reaction model by performing over 50 000 model calculations, each of which corresponds to

© 2023 The Authors. Advanced Energy Materials published by Wiley-VCH GmbH

16146840, 2023, 14, Downloaded from https://onlinelibrary.wiley.com/doi/10.1002/aenm.202203966 by Karlsruher Inst F. Technologie, Wiley Online Library on [11/07/2023]. See the Terms and Conditions (https://onlinelibrary.wiley.com/terms-and-conditions) on Wiley Online Library for rules of use; OA articles are governed by the applicable Creative Commons License

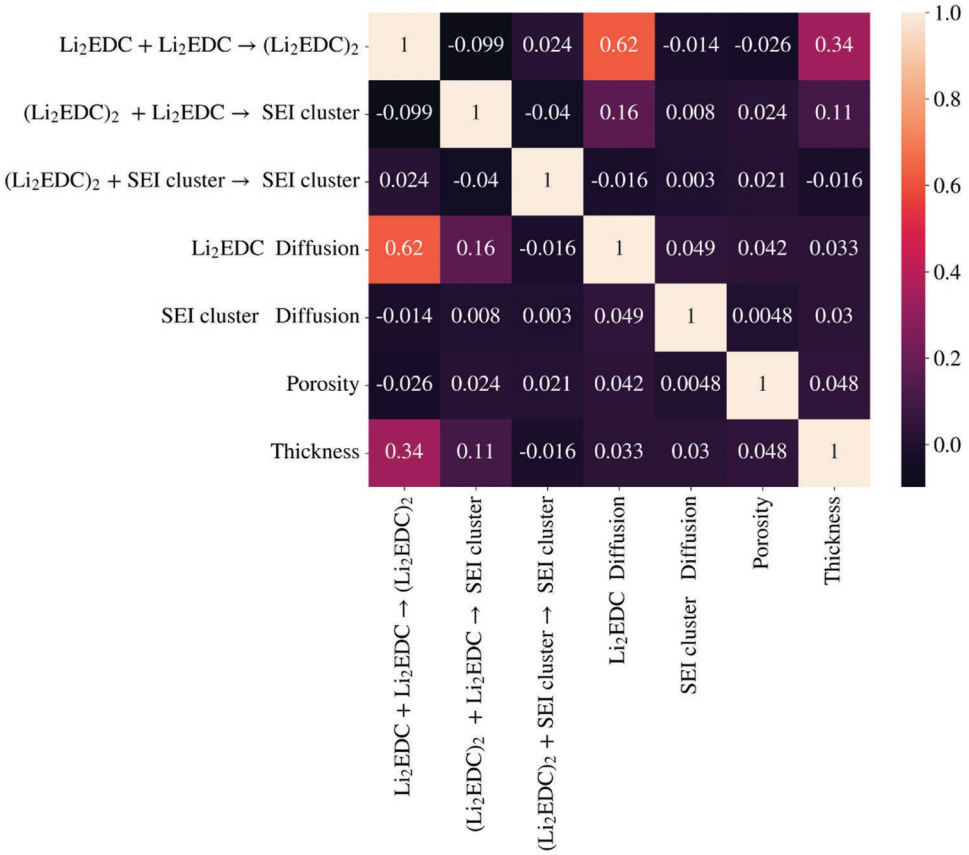

Figure 9. Correlation matrix plot of a few barriers (for reaction 5, 6, 9, 13, 15) and observables (SEI thickness and porosity) where 0 is for no linear correlation, and any positive and negative values indicate the positive and negative linear correlation between two variables. The formation of $(Li_2EDC)_2$ has a critical correlation with diffusion of Li_2EDC and thickness of the SEI.

a particular set of microscopic parameters. The model was chosen to balance the realism in the represented mechanisms with the computational feasibility. Analyzing all of these simulations we found that the resulting SEI-outcomes could be clustered in three regions, which we termed "inorganic", "bad", and "good" SEI.

Only for parameter sets in the latter region, we could observe the growth of a thick and stable SEI that eventually covers the surface of the electrode. In all of these simulations the SEI grew as a consequence of a nucleation reaction of SEI precursors that did not occur directly on the surface of the electrode, as postulated by most existing models, but far away from the surface in a solution-mediated pathway. We find a positive correlation between the thickness of the SEI and the distance from the electrode, where this nucleation reaction occurred. We conclude, surprisingly, that the most stable SEI is grown when the nucleation reaction occurs far from the surface. It is a consequence of this solution-mediated pathway that part of the degraded electrolyte diffuses far away from the surface and is lost for SEI formation. However, the fraction of mass-loss hovered around 20% of the degraded electrolyte precursors. We could identify the reaction that leads to the formation of $(Li_2EDC)_2$ as the essential prerequisite for the nucleation reaction, which offers an insight into an experimentally controllable reactions to design the properties of the SEI. SEI formed by a solution-mediated pathway will have significantly different electrochemical and mechanical properties from SEI that is grown in a continuous fashion starting at the electrode and progressing towards the electrolyte. Our model offers the opportunity to investigate these properties by using the outcome of our simulations for functional studies of batteries. The SEI depicted in Figure 1f can be further analyzed with respect to Li ion diffusion during charging/discharging. The organic SEI is much more porous than the inorganic SEI, which has consequences for long-term battery operation. With each charging cycle, the soft organic SEI is expected to crack which will result in further degradation of solvent molecules. The latter process leads to the continuous irreversible consumption of active battery materials and ultimately limits the lifetime of the battery.

It is interesting to compare our simulation results with experimental observation. Presently only qualitative comparison is warranted. **Figure 10**a, an extreme high resolution scanning electron microscopy (XHR-SEM) image of SEI after 5 min of ion etching on graphite electrode,[52] shows the morphology (thickness and porosity) of an SEI layer on graphite that is commensurate with the morphology of the SEI in region 3 in our simulation.

Both in experiment and simulation the morphology of the SEI is observed at the scale of about 40 nm (Figure 10b) and it comprises a dense inner and a more porous outer zone.[53] This

© 2023 The Authors. Advanced Energy Materials published by Wiley-VCH GmbH

16146840, 2023, 14, Downloaded from https://onlinelibrary.wiley.com/doi/10.1002/aenm.202203966 by Karlsruher Inst F. Technologie, Wiley Online Library on [11/07/2023]. See the Terms and Conditions (https://onlinelibrary.wiley.com/terms-and-conditions) on Wiley Online Library for rules of use; OA articles are governed by the applicable Creative Commons License

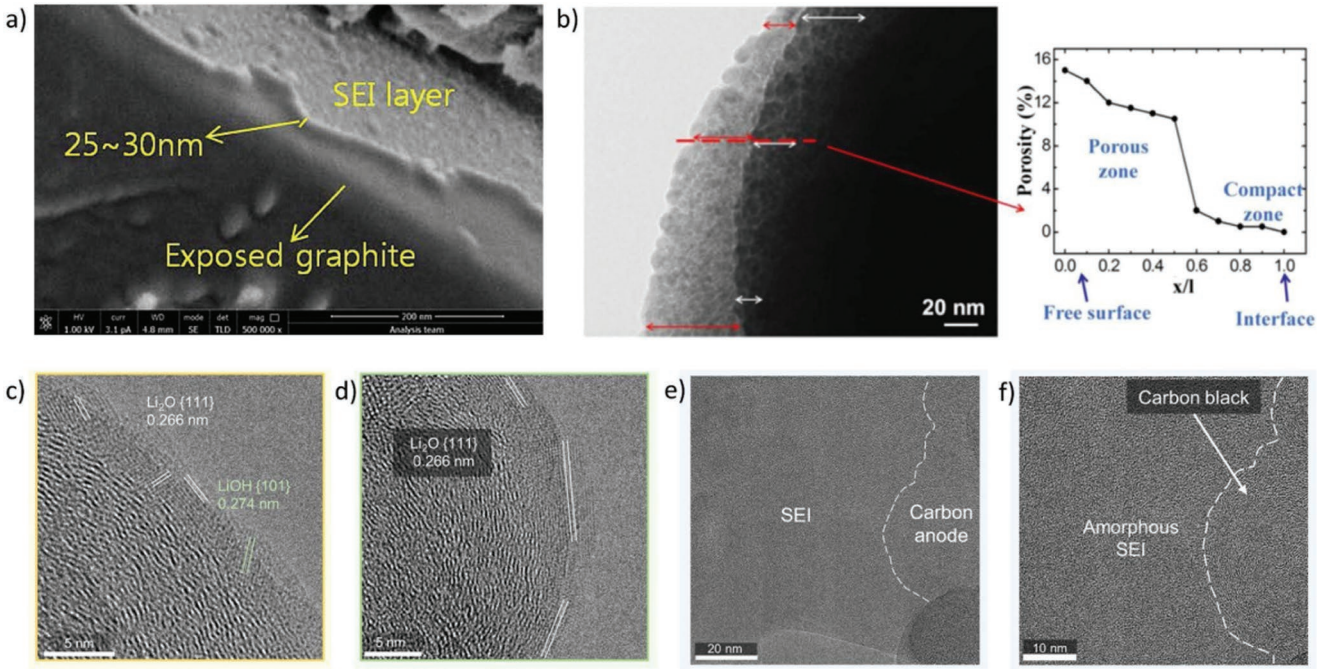

Figure 10. Images of SEI from experiments using advanced techniques (scanning electron microscopy (SEM), transmission electron microscopy (TEM)). a) XHR-SEM image of SEI layer on graphite electrode after 5 min of ion etching. Reproduced with permission.[52] Copyright 2013, Elsevier. b) The TEM image and the porosity analysis of the SEI layer. Reproduced according to the terms of the Creative Commons Attribution 4.0 license.[53] Copyright 2015, The authors, published by IOP. c,d) Cryo-TEM images of the compact SEI with an approximate thickness of 5 nm. e,f) Cryo-high-resolution transmission electron microscopy images of the extended SEI interfaced with carbon black. Reproduced with permission.[54] Copyright 2019, American Chemical Society.

finding is commensurate with the solution-mediated pathway scenario because the density of precursors that aggregate into the SEI decreases with the distance from the surface. A growth mechanism which starts at the surface would not produce a discontinuous porosity distribution as shown in Figure 10b. Finally, Figure 10c–f shows two examples of SEI representing the growth of the SEI under different conditions.[54] Figure 10c,d corresponds to a scenario, where only the inorganic SEI is growing, which corresponds to region 1 in our SEI landscape (inorganic SEI only), while Figure 10e,f corresponds to a scenario, where substantial growth of the SEI is observed, corresponding to the region we call "good SEI". At present this comparison is only indicative of possible scenarios, but it demonstrates that the mesoscopic model discussed here can yield SEI composition and properties in qualitatively in agreement with experimental observation. Future efforts shall try to make this correspondence more quantitative. We will also systematically test some of the assumptions that we had to make in this study. We will test whether a three-dimensional model will yield quantitatively different results, but we strongly expect that the two-dimensional model can capture the qualitative mechanism by which the organic SEI in LIBs is growing. While the present study is focused on the mechanism of SEI growth in general, future work can address different and more complex systems. Here, we see two avenues: where available we can use ab-initio data for other systems to directly parameterize the KMC simulations. Additionally, we can rely on molecular dynamics simulations on smaller time- and length scales as an intermediate model to parameterize the KMC.[55] The model can be easily extended to account for the presence of additives and mixtures of electrolytes. Again, the model will validate with experiments (X-ray photoelectron spectroscopy and TEM results for the SEI formation on the graphite anode from the BIG-MAP partners). Also, the input parameters will provide to refine the efficient continuum scale models with high accuracy to predict SEI properties along cycling in LIBs.

Supporting Information

Supporting Information is available from the Wiley Online Library or from the author.

Acknowledgements

The authors acknowledge the support from the BIG-MAP, funded by the European Union's Horizon 2020 Research and Innovation Program under Grant Agreement No. 957189. The project is part of BATTERY 2030+, the large-scale European research initiative for inventing the sustainable batteries of the future.

Open access funding enabled and organized by Projekt DEAL.

Conflict of Interest

The authors declare no conflict of interest.

Data Availability Statement

The data that support the findings of this study are available from the corresponding author upon reasonable request.

© 2023 The Authors. Advanced Energy Materials published by Wiley-VCH GmbH

16146840, 2023, 14, Downloaded from https://onlinelibrary.wiley.com/doi/10.1002/aenm.202203966 by Karlsruher Inst F. Technologie, Wiley Online Library on [11/07/2023]. See the Terms and Conditions (https://onlinelibrary.wiley.com/terms-and-conditions) on Wiley Online Library for rules of use; OA articles are governed by the applicable Creative Commons License

Keywords

interfacial reactivity, kinetic Monte Carlo simulation, lithium-ion batteries, machine learning, multiscale modeling, solid electrolyte interphase

Received: November 21, 2022
Revised: January 10, 2023
Published online: February 17, 2023

[1] D. Stampatori, P. P. Raimondi, M. Noussan, *Energies* **2020**, *13*, 2638.
[2] J. Wu, M. Ihsan-Ul-Haq, Y. Chen, J.-K. Kim, *Nano Energy* **2021**, *89*, 106489.
[3] L. Xie, C. Tang, Z. Bi, M. Song, Y. Fan, C. Yan, X. Li, F. Su, Q. Zhang, C. Chen, *Adv. Energy Mater.* **2021**, *11*, 2101650.
[4] M. Winter, *Z. Phys. Chem.* **2009**, *223*, 1395.
[5] J. B. Goodenough, Y. Kim, *Chem. Mater.* **2010**, *22*, 587.
[6] L. Wang, A. Menakath, F. Han, Y. Wang, P. Y. Zavalij, K. J. Gaskell, O. Borodin, D. Iuga, S. P. Brown, C. Wang, K. Xu, B. W. Eichhorn, *Nat. Chem.* **2019**, *11*, 789.
[7] T. Liu, L. Lin, X. Bi, L. Tian, K. Yang, J. Liu, M. Li, Z. Chen, J. Lu, K. Amine, K. Xu, F. Pan, *Nat. Nanotechnol.* **2019**, *14*, 50.
[8] D. Liu, Z. Shadike, R. Lin, K. Qian, H. Li, K. Li, S. Wang, Q. Yu, M. Liu, S. Ganapathy, X. Qin, Q.-H. Yang, M. Wagemaker, F. Kang, X.-Q. Yang, B. Li, *Adv. Mater.* **2019**, *31*, 1806620.
[9] A. Wang, S. Kadam, H. Li, S. Shi, Y. Qi, *npj Comput. Mater.* **2018**, *4*, 1.
[10] S. A. Delp, O. Borodin, M. Olguin, C. G. Eisner, J. L. Allen, T. R. Jow, *Electrochim. Acta* **2016**, *209*, 498.
[11] S. K. Heiskanen, J. Kim, B. L. Lucht, *Joule* **2019**, *3*, 2322.
[12] B. Horstmann, F. Single, A. Latz, *Curr. Opin. Electrochem.* **2019**, *13*, 61.
[13] Y. Gao, Z. Yan, J. L. Gray, X. He, D. Wang, T. Chen, Q. Huang, Y. C. Li, H. Wang, S. H. Kim, T. E. Mallouk, D. Wang, *Nat. Mater.* **2019**, *18*, 384.
[14] P. G. Kitz, P. Novák, E. J. Berg, *ACS Appl. Mater. Interfaces* **2020**, *12*, 15934.
[15] Y. Zhou, M. Su, X. Yu, Y. Zhang, J.-G. Wang, X. Ren, R. Cao, W. Xu, D. R. Baer, Y. Du, O. Borodin, Y. Wang, X.-L. Wang, K. Xu, Z. Xu, C. Wang, Z. Zhu, *Nat. Nanotechnol.* **2020**, *15*, 224.
[16] Z. Zhang, K. Smith, R. Jervis, P. R. Shearing, T. S. Miller, D. J. Brett, *ACS Appl. Mater. Interfaces* **2020**, *12*, 35132.
[17] A. Ge, D. Zhou, K.-i. Inoue, Y. Chen, S. Ye, *J. Phys. Chem. C* **2020**, *124*, 17538.
[18] S. Malmgren, K. Ciosek, R. Lindblad, S. Plogmaker, J. Kühn, H. Rensmo, K. Edström, M. Hahlin, *Electrochim. Acta* **2013**, *105*, 83.
[19] K. Ushirogata, K. Sodeyama, Y. Okuno, Y. Tateyama, *J. Am. Chem. Soc.* **2013**, *135*, 11967.
[20] N. Takenaka, Y. Suzuki, H. Sakai, M. Nagaoka, *J. Phys. Chem. C* **2014**, *118*, 10874.
[21] L. Alzate-Vargas, S. M. Blau, E. W. C. Spotte-Smith, S. Allu, K. A. Persson, J.-L. Fattebert, *J. Phys. Chem. C* **2021**, *125*, 18588.
[22] S. Bertolini, P. B. Balbuena, *J. Phys. Chem. C* **2018**, *122*, 10783.
[23] J. L. Christensen, J. Newman, *J. Electrochem. Soc.* **2003**, *151*.
[24] L. von Kolzenberg, A. Latz, B. Horstmann, *ChemSusChem* **2020**, *13*, 3901.
[25] J. R. Winkler, H. B. Gray, *J. Am. Chem. Soc.* **2014**, *136*, 2930.
[26] K. Ushirogata, K. Sodeyama, Z. Futera, Y. Tateyama, Y. Okuno, *J. Electrochem. Soc.* **2015**, *162*, A2670.
[27] A. M. Andersson, A. Henningson, H. Siegbahn, U. Jansson, K. Edström, *J. Power Sources* **2003**, *119*, 522.
[28] B. Han, Y. Zou, G. Xu, S. Hu, Y. Kang, Y. Qian, J. Wu, X. Ma, J. Yao, T. Li, Z. Zhang, H. Meng, H. Wang, Y. Deng, J. Li, M. Gu, *Energy Environ. Sci.* **2021**, *14*, 4882.
[29] M. Nie, D. P. Abraham, Y. Chen, A. Bose, B. L. Lucht, *J. Phys. Chem. C* **2013**, *117*, 13403.
[30] H. J. Ploehn, P. Ramadass, R. E. White, *J. Electrochem. Soc.* **2004**, *151*, A456.
[31] M. B. Pinson, M. Z. Bazant, *J. Electrochem. Soc.* **2012**, *160*, A243.
[32] M. Tang, S. Lu, J. Newman, *J. Electrochem. Soc.* **2012**, *159*, A1775.
[33] F. Single, B. Horstmann, A. Latz, *J. Electrochem. Soc.* **2017**, *164*, E3132.
[34] M. Broussely, S. Herreyre, P. Biensan, P. Kasztejna, K. Nechev, R. Staniewicz, *J. Power Sources* **2001**, *97*, 13.
[35] J. Christensen, J. Newman, *J. Electrochem. Soc.* **2004**, *151*, A1977.
[36] A. B. Bortz, M. H. Kalos, J. L. Lebowitz, *J. Comput. Phys.* **1975**, *17*, 10.
[37] E. R. Bittner, *J. Am. Chem. Soc.* **2006**, *128*, 17156.
[38] Y. Wang, S. Nakamura, M. Ue, P. B. Balbuena, *J. Am. Chem. Soc.* **2001**, *123*, 11708.
[39] T. Eriksson, A. M. Andersson, A. G. Bishop, C. Gejke, T. Gustafsson, J. O. Thomas, *J. Electrochem. Soc.* **2001**, *149*, A69.
[40] K. Ushirogata, K. Sodeyama, Y. Okuno, Y. Tateyama, *J. Am. Chem. Soc.* **2013**, *135*, 11967.
[41] Y. Wang, S. Nakamura, M. Ue, P. B. Balbuena, *J. Am. Chem. Soc.* **2001**, *123*, 11708.
[42] K. Miyabe, R. Isogai, *J. Chromatogr. A* **2011**, *1218*, 6639.
[43] M. D. McKay, in *Proceedings of the 24th Conference on Winter Simulation - WSC '92*, ACM Press, New York **1992**, https://doi.org/10.1145/167293.167637.
[44] R. L. Iman, scpl/scpatin hypercube sampling, **2014**.
[45] A. Olsson, G. Sandberg, O. Dahlblom, *Struct. Safety* **2003**, *25*, 47.
[46] S. Lloyd, *IEEE Trans. Inf. Theory* **1982**, *28*, 129.
[47] S. Mannor, X. Jin, J. Han, X. Jin, J. Han, X. Jin, J. Han, X. Zhang, in *Encyclopedia of Machine Learning*, Springer, New York **2011**, pp. 563–564. https://doi.org/10.1007/978-0-387-30164-8_425.
[48] L. McInnes, J. Healy, J. Melville, *arXiv preprint arXiv:1802.03426* **2018**.
[49] M. A. Syakur, B. K. Khotimah, E. M. S. Rochman, B. D. Satoto, *IOP Conf. Ser.: Mater. Sci. Eng.* **2018**, *336*, 012017.
[50] D. Marutho, S. H. Handaka, E. Wijaya, Muljono, in *2018 International Seminar on Application for Technology of Information and Communication*, IEEE, Piscataway, NJ **2018**. https://doi.org/10.1109/isemantic.2018.8549751.
[51] K. R. Shahapure, C. Nicholas, in *2020 IEEE 7th International Conference on Data Science and Advanced Analytics (DSAA)*, IEEE, Piscataway, NJ **2020**, https://doi.org/10.1109/dsaa49011.2020.00096.
[52] S.-H. Lee, H.-G. You, K.-S. Han, J. Kim, I.-H. Jung, J.-H. Song, *J. Power Sources* **2014**, *247*, 307.
[53] P. Guan, L. Liu, X. Lin, *J. Electrochem. Soc.* **2015**, *162*, A1798.
[54] W. Huang, P. M. Attia, H. Wang, S. E. Renfrew, N. Jin, S. Das, Z. Zhang, D. T. Boyle, Y. Li, M. Z. Bazant, B. D. McCloskey, W. C. Chueh, Y. Cui, *Nano Lett.* **2019**, *19*, 5140.
[55] J. W. Abbott, F. Hanke, *J. Chem. Theory Comput.* **2022**, *18*, 925.

© 2023 The Authors. Advanced Energy Materials published by Wiley-VCH GmbH

16146840, 2023, 14, Downloaded from https://onlinelibrary.wiley.com/doi/10.1002/aenm.202203966 by Karlsruher Inst F. Technologie, Wiley Online Library on [11/07/2023]. See the Terms and Conditions (https://onlinelibrary.wiley.com/terms-and-conditions) on Wiley Online Library for rules of use; OA articles are governed by the applicable Creative Commons License